JOURNAL OF MATERIALS SCIENCE 28 (1993) 2536–2544

The microstructure of a Nicalon/SiC composite and fibre deformation in the composite

X. YANG, R. J. YOUNG
Polymer Science and Technology Group, Manchester Materials Science Centre, UMIST/University of Manchester, Grosvenor Street, Manchester M1 7HS, UK

The microstructure of a Nicalon/SiC composite has been examined in detail using electron microscopy. The microstructure of the fibres does not change significantly during fabrication of the composite. It was found that there were two kinds of SiC grains in the matrix, polyhedral-shaped ones near to the fibres with a size ranging from 10–100 nm and columnar grains, further away from the fibres and up to 500 nm in length. It was also found that there is an interfacial layer of thickness about 100 nm between the fibres and the matrix. Fibre deformation was followed using Raman spectroscopy. Well-defined Raman spectra could be obtained from free-standing fibres and the fibres and the matrix in the composite. It was found that for free-standing fibres, the 1350 cm^{-1} Raman band shifts to lower frequency during tensile deformation. In the composite, the same band shifts to lower frequency during axial compressive deformation indicating that the fibres are in tension while the composite is subjected to overall compression. It is suggested that this behaviour is consistent with the woven arrangement of Nicalon fibres in the composite.

1. Introduction

Silicon carbide has excellent heat stability, good strength at high temperature, high resistance to oxidation and low density, which make it an important candidate for use in high-temperature structural materials. However, monolithic silicon carbide is very brittle and has very low resistance to mechanical and thermal shock. Silicon carbide fibre reinforcement has recently been used to toughen the monolithic ceramic, with the composite being fabricated using the chemical-vapour infiltration methods [1–3]. The SiC fibre/SiC composite maintains the high-temperature advantages of the ceramic whilst overcoming its mechanical weakness. A number of papers have been published concerning the mechanical and thermal properties of this composite [4–11], but the microstructure of the material has received rather less attention. It is clear that the fibre distribution in the material, the microstructure and interfacial properties will be the main factors affecting the mechanical properties of the composite. In this present study the microstructure of a Nicalon fibre-reinforced silicon carbide (Nicalon/SiC) composite has been investigated using mainly transmission electron microscopy, with particular attention being directed towards the fibre/matrix interface. Fracture surfaces have been investigated using scanning electron microscopy, which provides information about fibre and matrix structure, interfacial properties, as well as the microstructure of the composite.

It is known that Raman spectroscopy can be employed to follow fibre deformation in fibre-reinforced resin composites. Both unidirectional composites with continuous fibres and model single fibre composites have been investigated for a variety of systems which include carbon fibre/PEEK[12, 13], polydiacetylene fibre/epoxy[14, 15], Kevlar/epoxy[16, 17], poly(p-phenylene benzobisthiazole (PBT) fibre/epoxy [18], and carbon fibre/epoxy resin systems [17]. Recently, in our group the residual fibre strain in a unidirectional continuous silicon carbide fibre-reinforced glass (Nicalon/glass) composite has been measured successfully using the technique [19]. So far, to our knowledge, no other technique for the investigation of fibre strain in such composites has been reported. In the present work the deformation of fibres in a woven two-directional fibre-reinforced Nicalon/SiC composite subjected to compressive load has been examined using Raman spectroscopy. The findings have been related to the microstructure and fracture behaviour of the composite.

2. Experimental procedure

2.1. Materials

The Nicalon/SiC composite used in the study was supplied by Du Pont. It consists of a woven two-directional continuous Nicalon fibre fabric layer reinforcing a silicon carbide ceramic matrix. It was supplied in the form of plates with a thickness of 2.8 mm. The surface appearance of the material is shown in Fig. 1 and it has a similar surface morphology to that of chemical-vapour deposited SiC materials [20]. Fig. 2 shows an optical micrograph of a polished cross-section of the material, revealing a cross-section of the warp yarn, a longitudinal section of the weft yarn and the matrix. It can be seen from the

0022–2461

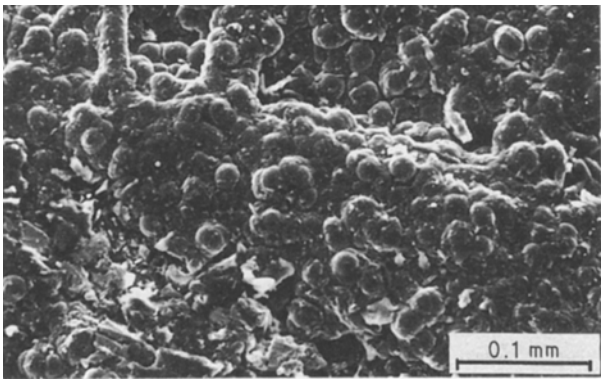

Figure 1 Scanning electron micrograph of the surface morphology of the SiC matrix of the Nicalon/SiC composite.

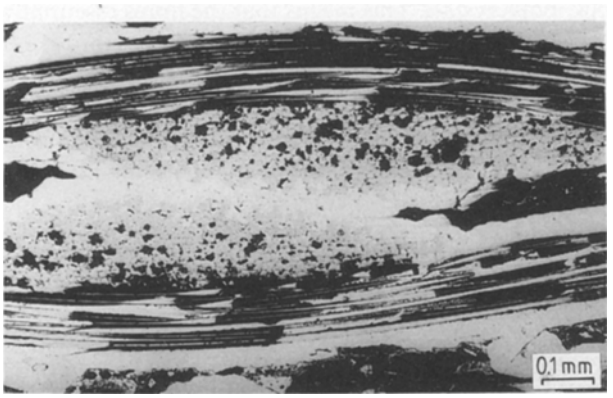

Figure 2 Optical micrograph of a polished cross-section of the composite.

micrograph that the silicon carbide matrix is uniformly deposited within the gaps between fibres in the yarns. However, it can also be seen that there are a number of voids between fabric layers and between the fibre bundles which were not filled with matrix during fabrication and also a number of large macroscopic voids present in the composite.

2.2. Electron microscopy

Philips 301 and 400T transmission electron microscopes (TEM) were used for the examination of the microstructure of the composite. Bright-field (BF) image, dark-field (DF) image and selected-area electron diffraction (SAD) modes were employed in the study. The thin foil specimens for TEM investigations were prepared using ion-beam thinning. A thin section of about 0.3 mm thickness was cut from the composite using an Isomet Diamond wafering blade so that the fabric layers were aligned parallel to the section. The section was then polished mechanically down to about 60 μm. An area of $3 \times 3\ mm^2$ was cut using a sharp blade and the section was fixed on a grid with a hole using an adhesive. Thinning was performed using a TECH 791 ion-beam thinning machine. A very thin carbon film was evaporated on the ion-thinned specimen to prevent electron-beam charging effects in the electron microscope.

A Philips EM505 scanning electron microscope (SEM) was used to examine the fracture surfaces after specimens had been deformed in compression as described in the next section. All specimens were coated with a thin layer of gold in a sputter-coating unit prior to observation to avoid charging in the microscope.

2.3. Raman spectroscopy

A Raman microscope system was used in the study. This consisted of a SPEX 1403 double monochromator with a charge-coupled device (CCD) camera connected a modified Nikon optical microscope. A 488 nm argon-ion laser was used to excite the Raman spectra.

Raman spectra were obtained from both the Nicalon fibres and the SiC matrix in the composite. The cross-section of the composite was polished to expose the fibres within the composite prior to the measurement because the silicon carbide matrix is opaque using visible light. The polishing was conducted using diamond polishing compound (Metadi II). The Raman spectra of Nicalon fibres obtained in this case were from the interior of the fibres, rather than being obtained from fibre surfaces as was done previously [19]. For comparison purposes, Raman spectra were obtained from free-standing Nicalon fibres in air and from polished sections of the same fibres in an epoxy resin matrix cured at room temperature.

Raman spectra were obtained from longitudinal sections of the fibres in the composites subjected to compressive load using a Polymer Laboratories Minimat mechanical testing machine which fitted directly on the Raman microscope stage. It was found that for the Nicalon SiC composites, compressive deformation was experimentally easier to undertake than tensile straining. Fig. 3 is a schematic diagram of the samples used for compression testing. The dimension of the samples was about $2.8 \times 3.0 \times 9.5\ mm^3$. The samples were positioned such that the direction of the weft yarn, was aligned parallel to the applied compressive load and the direction of laser-beam polarization. Surface A (Fig. 3) was polished to expose the fibres to the incident laser beam. The fibre sections of both the weft and warp yarns corresponding to longitudinal and cross-sections of the fibres, respectively, could be seen using the optical microscope attached to the system. The laser beam was focused on the peak of the

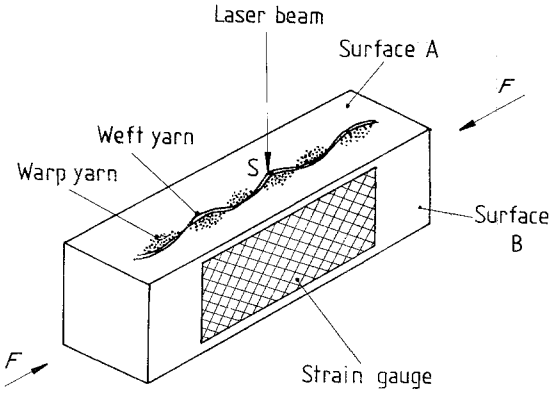

Figure 3 Schematic diagram of the composite specimen subjected to a compressive load, *F*.

wave form of fibres in the weft yarn, marked S in the figure. Surface B was also polished to allow a strain gauge to be applied to the sample surface.

3. Results and discussion

3.1. Microstructure

The microstructural investigations were mainly concentrated upon the crystalline phases of both the matrix and fibres and upon the interface between the fibres and the matrix. It is well known that interfacial phenomena, such as stress transfer from matrix to fibres, play a vital role in controlling the efficiency of fibre reinforcement. The phenomena depend upon the bonding between fibres and matrix. Therefore, particular attention was directed towards characterizing interfacial regions in the composite.

A typical TEM BF image micrograph of the composite is shown in Fig. 4a. The micrograph shows a fibre, the matrix and the interfacial region, referred to as F, M, and I, respectively. It can be seen from the figure that the BF image does not reveal any microstructural detail for the Nicalon fibres (region F) in the composite, as reported by the authors [19] and other workers [20]. A SAD pattern from the fibre is shown in Fig. 4b. Three rings can be seen in the pattern, corresponding to the SiC_{111}, SiC_{222} and SiC_{311} diffracted beams, respectively. The pattern indicates a high degree of polycrystallinity, a relatively small crystal size and a lack of preferred orientation for the SiC component of the fibres. In the pattern there is no evidence of free carbon, although it will be shown later that the Raman spectra of the fibres are dominated by broad Raman bands from carbon. A DF image from the same region at high magnification is shown in Fig. 5, revealing small crystals of SiC with sizes ranging from 3–4 nm. It appears from results described above that the microstructure of the Nicalon fibres in the composite is similar to that of the original fibre reported by the authors [19] and other workers [21–25], except for a small increase in the grain size of SiC polycrystals. This means that the fibres essentially retain their original microstructure during fabrication of the composite.

Fig. 4a reveals that the microstructural features of the SiC matrix (region M) are quite different from those of the SiC fibres with the matrix being made up of a number of larger SiC grains. It can be seen that the grains have a polyhedral shape in the region near the interface (region I) and are randomly arranged with no

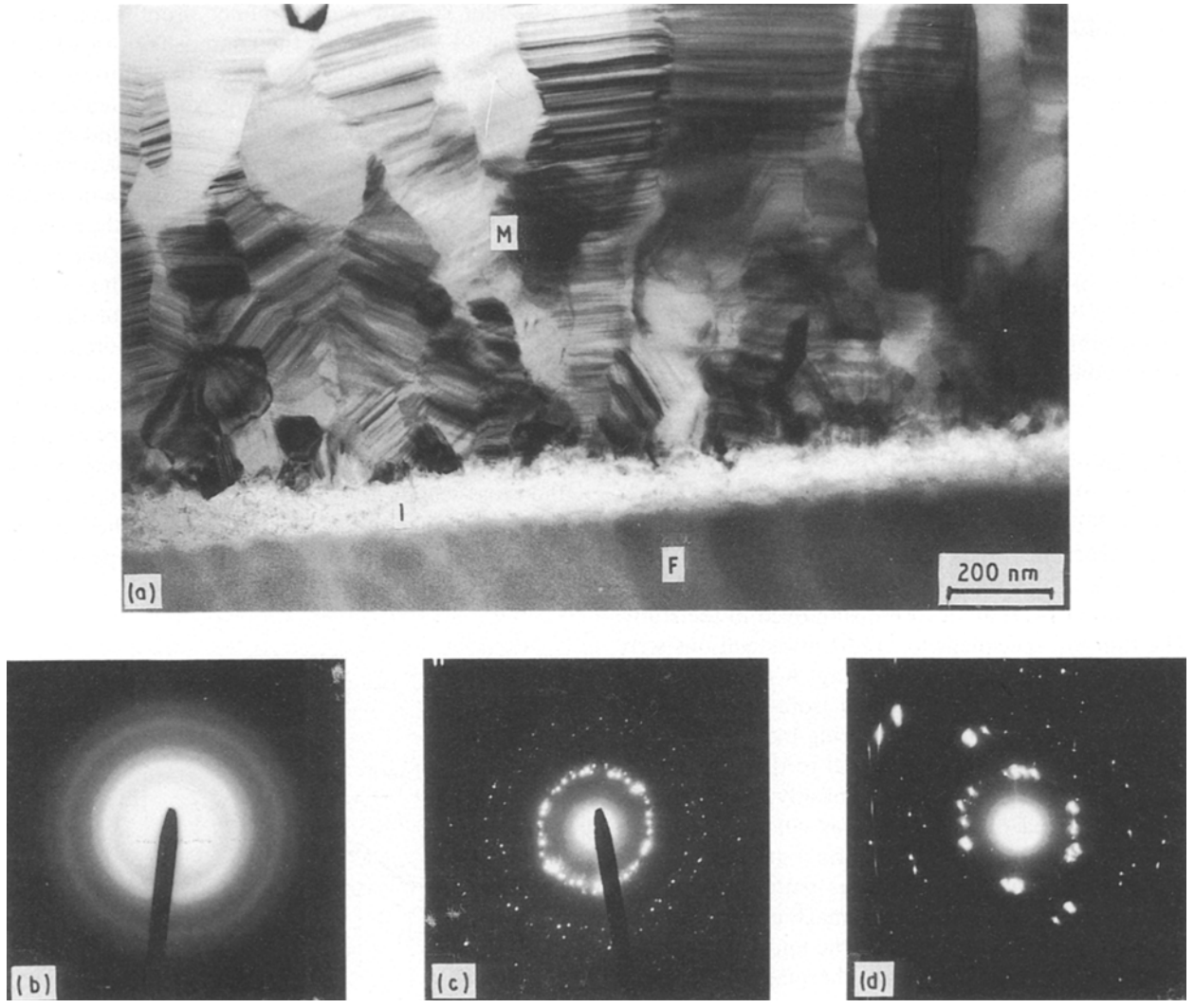

Figure 4 (a) A typical transmission electron micrograph of the composite showing the fibre (F), interface (I) and matrix (M) regions. (b–d) Selected-area electron diffraction patterns of (b) the fibre and (c, d) matrix regions in the micrograph.

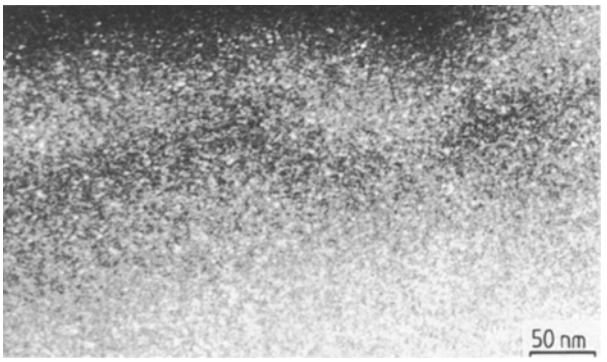

Figure 5 Dark-field TEM image of the Nicalon fibre in the composite.

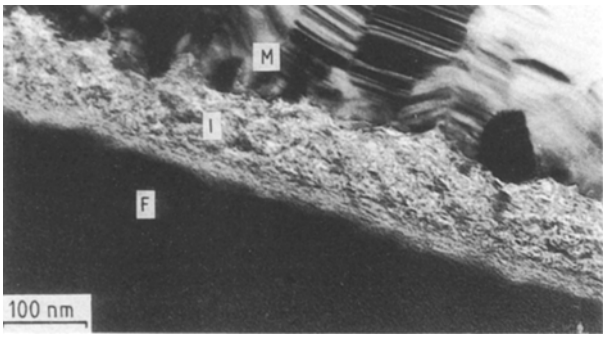

Figure 6 Transmission electron micrograph of the fibre/matrix interface at high magnification. (F = fibre; M = matrix; I = interface).

preferred orientation. The grains are analogous to the equiaxed grains which appear in the initial stage of chemical-vapour deposition of silicon carbide as reported by Shimozaki and Kinsman [26]. The grain size in the region ranges from several tens of nanometres near to the interface to more than 100 nm away from the interface. There is a clear boundary between the matrix and region I and some of the SiC grains protrude into region I. The SAD pattern of the SiC matrix close to the interfacial region is shown in Fig. 4c. It can be seen from the pattern that the rings from the SiC crystals consist of spots because there are insufficient grains in the SAD aperture (0.5 μm) to give complete rings in the diffraction pattern. There is no trace of preferred crystal orientation in the pattern, consistent with the arrangement of the grains revealed in the BF image of the matrix near to the interface (Fig. 4a).

In the region further away from the interface, the grains have a columnar shape being about 100 nm diameter and up to more than 500 nm long, and so are larger than that for the grains near the interface. The orientation of these columnar grains is clear. Almost all of the grains in the region contain the high density of narrow twins with the twin lamellae running completely across the grain diameter. Most twin lamellae are aligned approximately parallel to the interface, showing a preferred orientation between adjacent grains. A SAD pattern of the region is shown in Fig. 4d, revealing intensive arcing of the 1 1 1 reflections of the SiC crystals indicating a preferred orientation of the SiC grains, consistent with the arrangement of the grains revealed in the micrograph (Fig. 4a). Streaking is also present in the diffraction pattern, caused by extensive planar disorder within the grains. The variation of the microstructure of SiC grains from the matrix with distance from the interface is probably related to the fabrication process of the composite.

Region I in Fig. 4a shows an interface between a Nicalon fibre and the SiC matrix with thickness of about 100 nm. The detailed structure of the interface is shown in Fig. 6, a higher magnification transmission electron micrograph. It is seen from the figure that the interface has a fine granular structure with a grain size of up to 10 nm. Identification of the structure of this interfacial phase is difficult because it is so thin and the structure of this region is the subject of current investigation. It is known, however, that carbon is often deposited on the fibres before deposition of the SiC matrix. It can also be seen that there is a very clear boundary between the matrix and the interfacial layer but the boundary between the fibre and the interface is not so well defined. Other kinds of structural features at the interface were also found by TEM observation as shown in Fig. 7. In this case there is no definite interfacial boundary layer but rather a gradient in size of the polyhedral SiC grains, varying from about 10 nm in the region near the fibres to about 100 nm in the region far away from the fibres. It is clear, therefore, that the interfacial layers may not be very uniform in structure. The SAD pattern also indicated no preferred orientation for these SiC grains.

Fig. 8 shows BF images and corresponding DF images using the 1 1 1 diffracted beam for polyhedral (Fig. 8a and b) and columnar (Fig. 8c and d) matrix SiC grains, respectively. These images again show the different structural features of the two kinds of matrix SiC grains.

The fact that there are significantly different structural features in the composite is reasonable because, in general, the conditions of the fabrication process vary over the processing time of the material and are not constant [1, 8], which means that the conditions under which the interfaces form alter during the fabrication process. For isothermal chemical vapour infiltration, however, which was used in the fabrication of the composites used in the present study, the conditions of the fabrication process were relatively constant. This indicates that the mechanism of interface formation is clearly quite complex. It will be a subject of further study, but it has been demonstrated above that the present approach is a powerful method of characterizing such composites.

It has been reported that pull-out tests [27, 28] and indentation tests [29] can be used to characterize the properties of the interface in fibre-reinforced ceramic composites, and interfacial friction or bonding have been mainly investigated. It is not possible to quantify the strength of the interface from TEM observation. It has been shown, however, that the SiC matrix and the interfacial material do not separate from the fibres during the process of specimen preparation (mechanical and ion-beam thinning). This means that the bond between the fibres and matrix must have some limited strength. However, the SEM observations of fracture

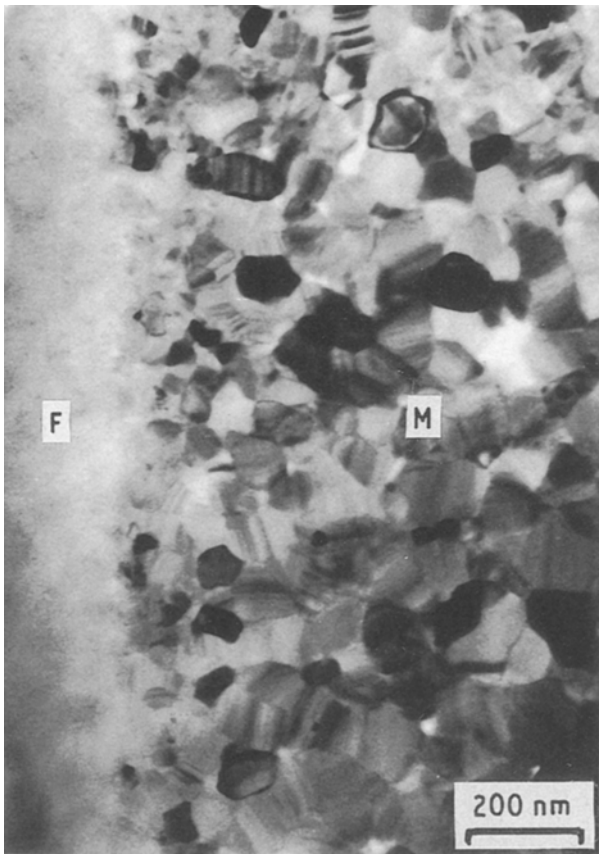

Figure 7 Transmission electron micrograph of the fibre/matrix interface showing no definite boundary. (F = fibre; M = matrix).

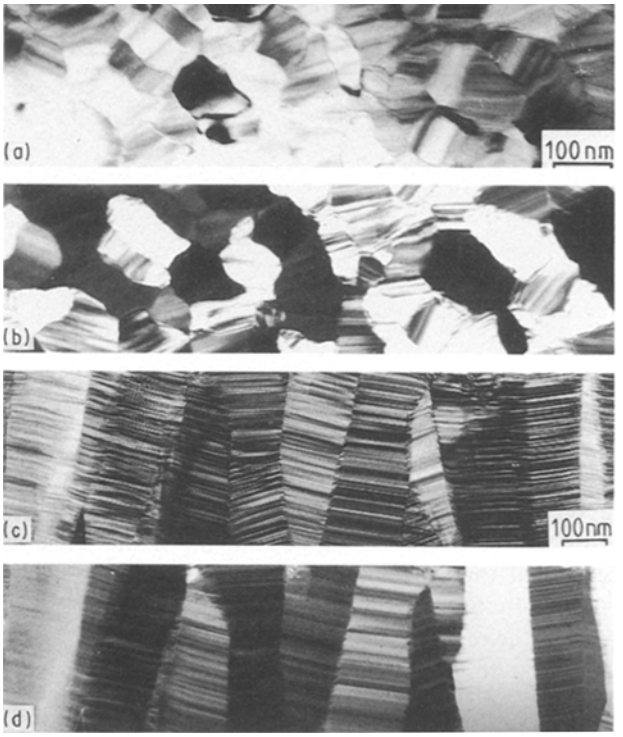

Figure 8 (a, c) Bright-field images and (b, d) corresponding dark-field images of the SiC matrix with polyhedral and columnar grains, respectively.

surfaces, to be described later, give a better idea of the strength of bonding at the interface.

3.2. Raman spectroscopy

Raman spectra could be obtained for both the Nicalon fibres and the SiC matrix in the composite using a suitable combination of laser power and exposure time. Typical spectra in the region 700–1720 cm^{-1} for the fibres and the matrix in the composite are shown in Fig. 9a and b, respectively. The Raman spectrum from the surface of a free-standing Nicalon fibre in air (Fig. 9c) and from the longitudinal section of the fibres in an epoxy resin (Fig. 9d) are also presented in the figure. It can be seen that the three spectra from the Nicalon fibres (Fig. 9a, c and d) all show three well-defined bands, 1350 and 1600 cm^{-1} bands due to the graphite and a 830 cm^{-1} band due to the SiC microcrystals. The spectrum from the longitudinal section of the fibre in the composite (Fig. 9a) and in the epoxy resin (Fig. 9d) are very similar, indicating that the significant change in the microstructure of the fibres did not take place during fabrication of the SiC composite. However, comparing the spectrum from the fibre-free surface (Fig. 9c) with those from longitudinal sections, both in the SiC composite (Fig. 9a) and in the resin (Fig. 9d), reveals some differences. The ratio of intensity of the 1350 cm^{-1} band to that of the 1600 cm^{-1} band for longitudinal section of the fibre in the SiC composite or in the epoxy resin is markedly lower than that for

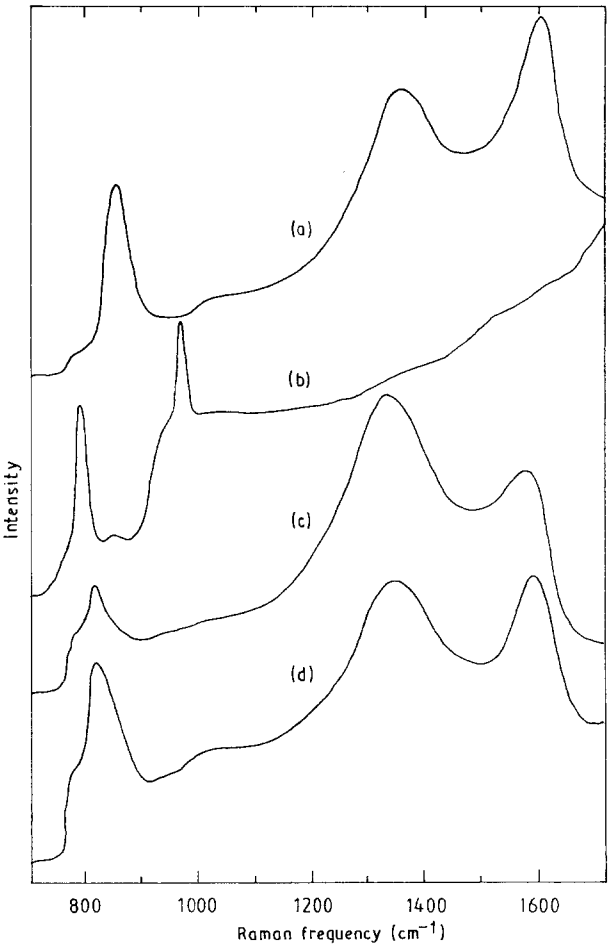

Figure 9 Raman spectra of (a) the Nicalon fibre, (b) the SiC matrix in the composite, (c) a free-standing fibre in air, and (d) a longitudinal section of a Nicalon fibre in an epoxy resin.

the surface of the fibre. This probably means that, in view of the findings of Tuinstra and Koenig [30] concerning the relationship between this ratio and the crystal size, the size of graphite crystals in the interior of the fibre is larger than that in the surface of the fibre. It can also be seen that the intensity of the 830 cm^{-1} band for the longitudinal sections of the fibre (Fig. 9a and d) is considerably higher than that for surface of the fibre (Fig. 9c), which may be due to the lower concentration of SiC in the surface region of the fibre.

The Raman spectrum for the SiC matrix (Fig. 9b) is quite different from those for the Nicalon fibre. No bands due to graphite appear in the spectrum, which indicates that there is very little free carbon in the SiC matrix. Two sharp bands, at 790 and 970 cm^{-1} appear in the SiC spectrum instead of the 830 cm^{-1} SiC band found for the Nicalon fibre. This is consistent with the findings for hot-pressure SiC [31], sintered SiC [31] and SiC crystals [32]. These two sharp bands can be attributed to the zone-centre transverse optical phonon (790 cm^{-1}) and the zone-centre longitudinal optical phonon (970 cm^{-1}), respectively, of crystalline SiC [33].

The Raman spectrum and the sensitivity of all three bands to applied strain for the Nicalon fibre in air have recently been examined in detail [19, 34]. In this present study, work has concentrated upon fibre deformation in the composite evaluated using the known dependence of the peak position of the 1350 cm^{-1} band upon applied strain for the fibre in air. Fig. 10a shows the Raman spectrum for a Nicalon fibre in the region 1100–1470 cm^{-1} in the undeformed state and subjected to a tensile strain of 1.6%. It can be seen that the band shifts to lower frequency with applied tensile strain. The relationship between the peak position of the band and strain is shown in Fig. 10b. There is a linear shift in frequency with strain until fibre failure occurs and the slope of the line is $-6.8\ cm^{-1}/\%$.

The effect of composite strain, e_c, upon the band positions for the fibre in the composite is shown in Fig. 11. It can be seen from Fig.11a that the band shifts to lower frequency with applied compressive strain. Fig. 11b shows that there is a linear relationship between the Raman frequency and the composite compressive strain for the 1350 cm^{-1} band with a slope of $-60\ cm^{-1}/\%$ composite compressive strain. A conclusion from this examination is that the fibres in the composite are subjected to tension while the composite is under axial compression, assuming that the dependence of the band position upon strain for the fibre surface in tension is also valid for fibre interior in compression. For example the local tensile strain for that part of the fibre being measured (the strain of fibre along fibre length might be not homogeneous) is 0.66%, while the compressive strain in the composite is 0.07%.

It has been shown previously that for a unidirectional composite with continuous fibres subjected to axial compression, the fibres undergo compressive deformation [18]. However, multidirectional composites with continuous fibres have more complex mechanical response [35] than unidirectional composites, because they have a complex network structure of fibre bundles. The composite used in the present study may be regarded as a network of impregnated fibre bundles rather than a continuous material because it has a porous structure as shown in Fig. 2 and, as will be described in the next section, relatively weak bonding between the fibres and matrix. The deformation and failure of the fibres are closely related to the distortion of the network and friction within the fibre bundles. Therefore, the occurrence of local tensile deformation in part of fibres through processes such as axial splitting and fibre bridging could be possible even though the structure is subjected to overall compression.

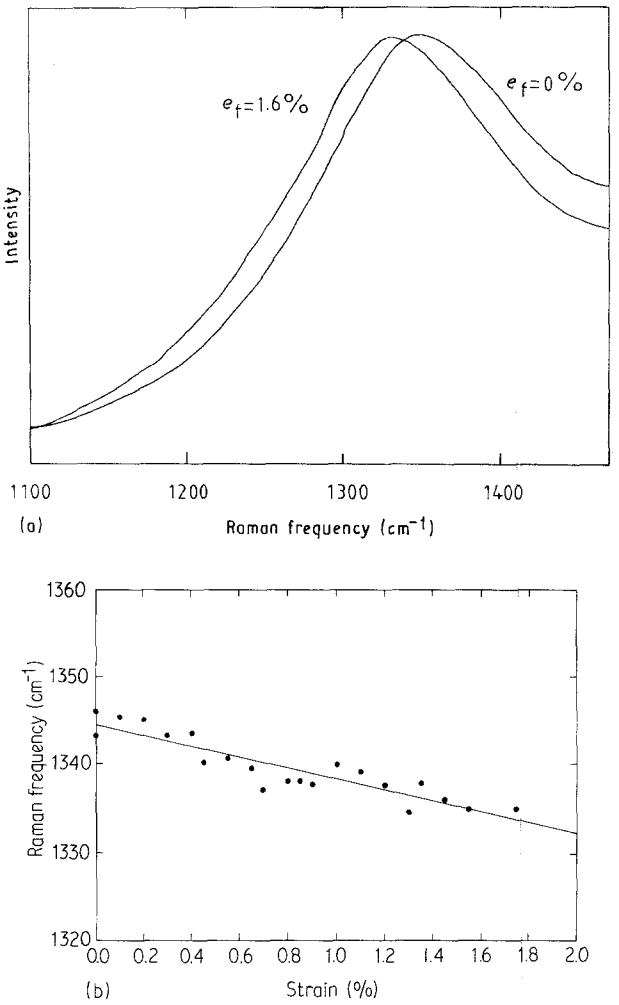

Figure 10 (a) Shift in the position of the 1350 cm^{-1} Raman band with strain for a free-standing Nicalon fibre. (b) Dependence of the peak position of the 1350 cm^{-1} Raman band upon applied strain for a free-standing Nicalon fibre.

3.3. Fracture morphology

The observation of fracture surfaces also provides information on microstructural features of composite and fibre deformation during composite failure. Fig. 12 shows a fracture surface of the composite after compressive failure by splitting parallel to the fabric laminates. It can be seen that virtually all of the fibres are coated with SiC matrix but that there are also gaps between the fibre bundles. Fig. 13 reveals two kinds of matrix morphology, granular material with grain size of about 10 μm, and bulk material with many small

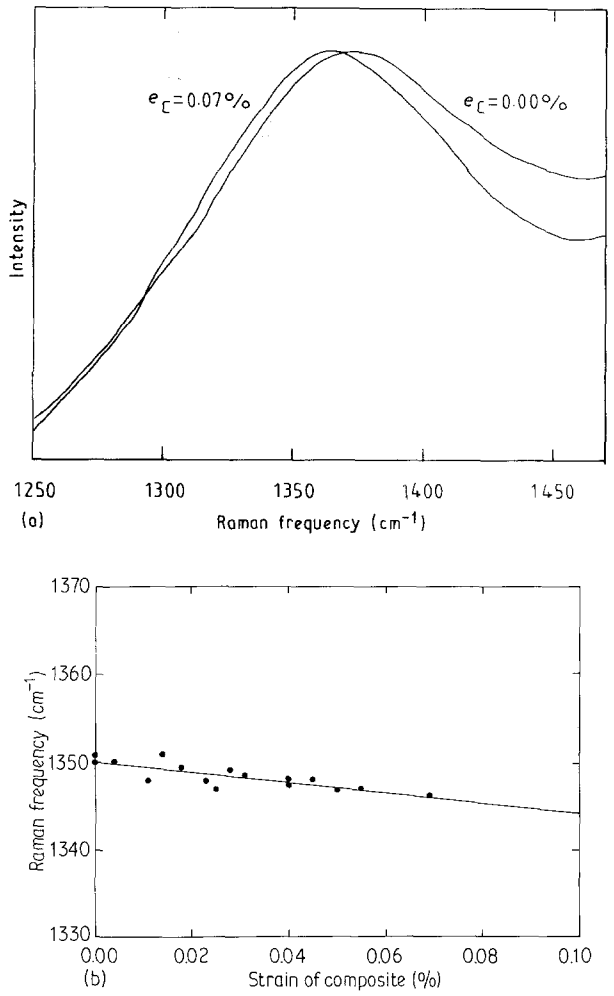

Figure 11 (a) Shift in the position of the 1350 cm^{-1} Raman band for a Nicalon fibre in the composite with overall compressive composite strain, e_c. (b) Dependence of the position of the 1350 cm^{-1} Raman band for the Nicalon fibres in the composite upon the applied axial strain.

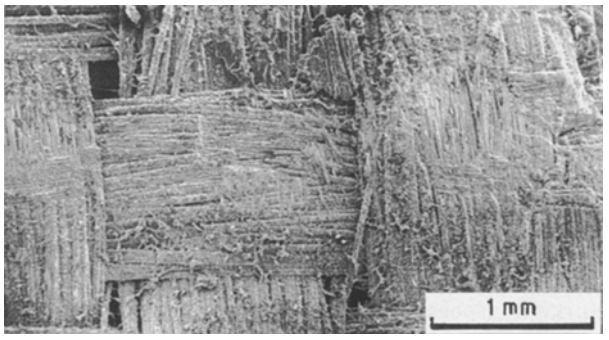

Figure 12 Scanning electron micrograph of the fracture surface caused by compressive failure, showing large voids and gaps between the fibre bundles.

pores about 1 μm in size. These microstructural features of the matrix are probably related to the composite fabrication process. Nevertheless, the pores, the gaps between the crystals and the cracks in matrix are thought to be of benefit for the achievement of high fracture toughness [8].

It is well known that SEM examination of fracture surfaces and of cracks near fracture surfaces can provide evidence of the various modes of failure in materials. Fig. 14 is a higher magnification micrograph of the fracture surface near one of the ends of the sample where load was applied. It can be seen that all of the likely modes of failure, such as delamination, fibre breakage, interface debonding and multicracking through the matrix, occur in the composite.

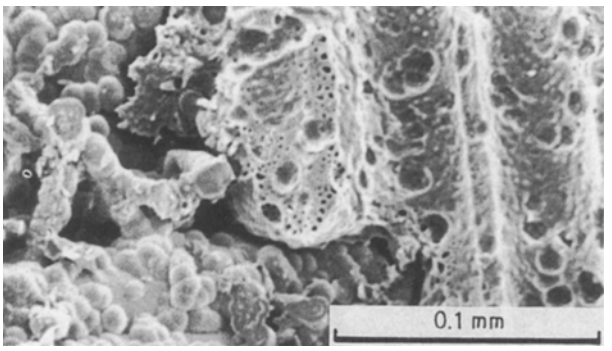

Figure 13 Scanning electron micrograph of the general morphology of the matrix.

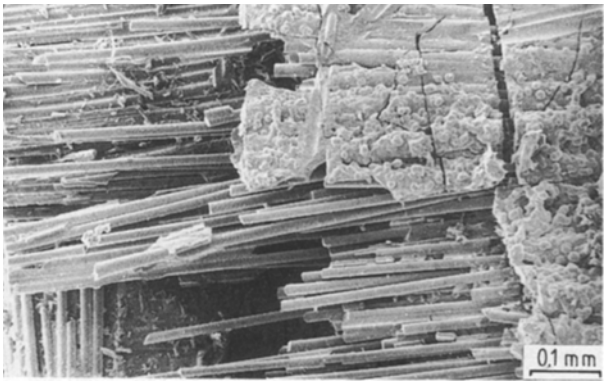

Figure 14 Scanning electron micrograph of the fracture surface showing fibre breakage, matrix cracking and debonding between fibres and matrix.

Fig. 15a shows a scanning electron micrograph of a polished surface of the composite (surface A, Fig. 3) following compressive failure. The cracks were not induced by the mechanical polishing but appeared following compressive failure. It can be seen that the cracks extend approximately along the weft yarn with some evidence of crack deflection. Fig. 15b is a higher magnification micrograph of part of Fig. 15a revealing debonding of the fibres in the warp yarn from the matrix. This is evidence of a weak fibre–matrix interface causing crack deflection. Fig. 15c is another micrograph of a local region of Fig. 15a at high magnification, showing evidence of fibre pull-out and fibre breakage in the weft yarn. These observations of the phenomena confirm that the fibres in this region (the peak of the wave-shaped fibres in weft yarn) may be subjected to tension during overall axial compression of the composite, consistent with the result from the Raman band-shift measurements.

4. Conclusions

1. The SiC component of the Nicalon fibres in the composite has a polycrystalline microstructure with a

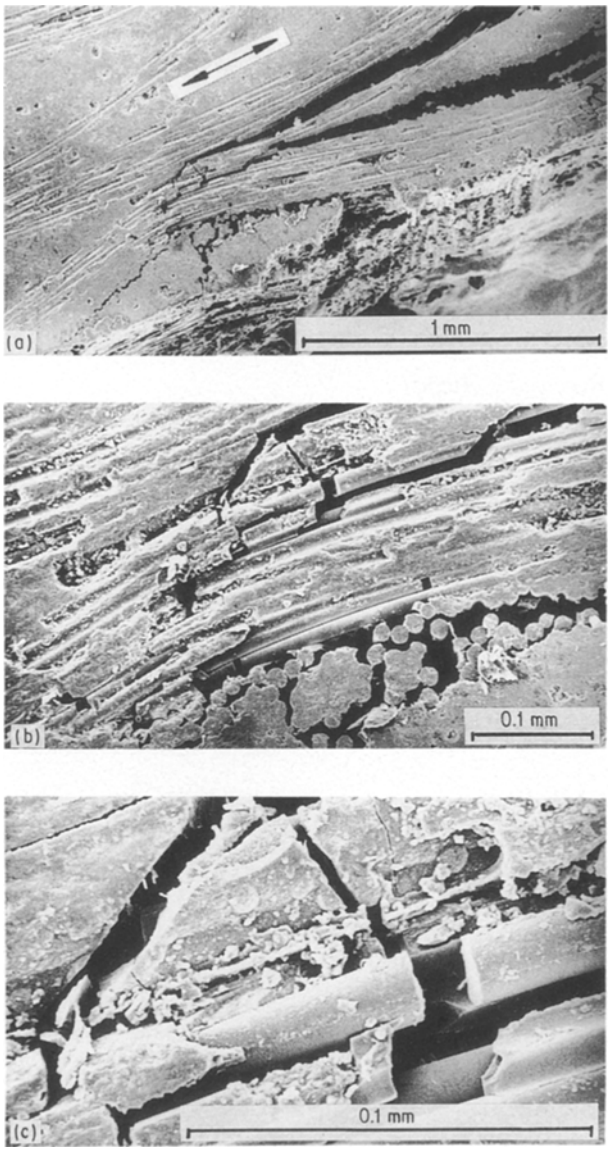

Figure 15 Scanning electron micrographs of a polished section following axial compression, showing (a) crack deflection. (b) debonding and (c) fibre pull-out and fibre breakage.

grain size ranging from 3–4 nm, slightly larger than that for the same fibres before fabrication into the composite. Examination of the SiC matrix reveals that there are two kinds of SiC crystalline grains, polyhedral-shaped grains near the fibres with a size ranging from 10–100 nm, and highly-twinned columnar grains further away from the fibres with size of about 100 nm in diameter and up to 500 nm long. There is an interfacial phase with a thickness of about 100 nm between the Nicalon fibres and the SiC matrix in the composite with a granular structure and a grain size of up to 10 nm.

2. The peak position of the 1350 cm^{-1} Raman band for the fibres deformed in tension in air shifts to lower frequency. The peak position of the band also shifts to lower frequency in the composite with applied composite compressive strain. Hence it appears that some of the fibres are in tension while the composite is subjected to overall compression.

3. Various modes of failure, including delamination, fibre breakage, interfacial debonding and multi-cracking through the matrix occur in the composite when it undergoes compressive failure. There is also evidence of fibre pull-out taking place during compressive failure, showing that there is relatively weak bonding between the fibres and matrix. Some of the fibres of the weft yarn which are approximately parallel to the compression direction, tend to break in tension, while some of the fibres of the warp yarn, which are oriented transverse to the loading direction, tend to debond from the matrix.

4. It appears approach adopted in this present study provides a unique method of following the deformation micromechanics of ceramic fibre-reinforced ceramic-matrix composites.

Acknowledgements

This work was supported by a research grant from the SERC. The authors thank Dr D. Roach, Du Pont, Wilmington, for supplying the Nicalon/SiC composite and for helpful comments on the manuscript.

References

1. D. P. STINTON, A. J. CAPUTO and R. A. LOWDEN, *Amer. Ceram. Soc. Bull.* **65** (1986) 347.
2. A. J. CAPUTON, D. P. STINTON, R. A. LOWDEN and I. M. BESMANN, *ibid.* **66** (1987) 268.
3. R. D. VELTRI, D. A. CONDIT and F. S. GALASSO, *J. Amer. Ceram. Soc.* **72** (1989) 478.
4. P. J. LAMISQ, G. A. BERNHART, M. M. DAUCHIER and J. G. MACE, *Amer. Ceram. Soc. Bull.* **65** (1986) 336.
5. M. M. DAUCHIER, G. A. BERHART and C. BONNET, in "Proceedings of the 30th National SAMPE Meeting" 1985 (SAMPE, Covina, 1985), pp. 1519.
6. A. J. ECKEL and R. C. BRADT, *J. Amer. Ceram. Soc.* **72** (1989) 455.
7. A. N. FRETY and M. BOUSSUGE, *Comp. Sci. Tech.* **37** (1990) 177.
8. R. KOCHENDORFER, in "4th European Conference on Composite Materials", Stuttgart, 1990, edited by J. Fuller, G. Gruninger, K. Schulte, H. R. Bunsell and A. Massiah (Elsevier Applied Science, London 1990) p. 685.
9. J. M. YANG, W. LIW, C. J. SHIH, W. KAI, S. M. JENG and C. B. BURKLAND, *J. Mater. Sci.* **26** (1991) 2954.
10. E. INGHELS and J. LAMON, *ibid.* **26** (1991) 5403.
11. *Idem, ibid.* **26** (1991) 5411.
12. R. J. YOUNG, R. J. DAY, M. ZAKIKHANI and I. M. ROBINSON, *Compos. Sci. Tech.* **34** (1989) 243.
13. C. GALIOTIS, J. A. PEACOCK, D. N. BATCHELDER and I. M. ROBINSON, *Composites* **19** (1988) 321.
14. C. GALIOTIS, R. J. YOUNG, P. H. J. YEUNG and D. N. BATCHELDER, *J. Mater. Sci.* **19** (1984) 3640.
15. I. M. ROBINSON, R. J. YOUNG, C. GALIOTIS and D. N. BATCHELDER, *ibid.* **22** (1987) 3642.
16. C. GALIOTIS, I. M. ROBINSON, D. N. BATCHELDER and R. J. YOUNG, in "Engineering Applications of New Composites", edited by S. A. Paipetis and G. C. Papanicolaou (Omega Scientific, Wallingford, 1988), p. 409.
17. C. GALIOTIS, *Compos. Sci. Tech.* **42** (1991) 125.
18. R. J. YOUNG and P. P. ANG, in "4th European Conference on Composite Materials", Stuttgart 1990, edited by J. Fuller, G. Gruninger, K. Schulte, A. R. Bunsell and A. Massiah (Elsevier Applied Science, London, 1990) p. 685.
19. X. YANG and R. J. YOUNG, to be published.
20. S. S. SHINOZAKI and H. SOTO, *J. Amer. Ceram. Soc.* **61** (1978) 425.
21. Y. MANIETT and A. OBERLIN, *J. Mater. Sci.* **24** (1989) 3361.
22. *Idem. ibid.* **25** (1990) 3864.

23. A. R. BUNSELL, "Fibre Reinforcement for Composite Materials", (Elsevier, Amsterdam, 1988), Ch. 9.
24. L. C. SAWYER, R. ARONS, F. HAIMBACK, M. JAFFE and K. D. RAPPAPORT, in "Proceedings of the 9th Annual Conference on Composites and Advanced Ceramic Materials", Program Chair: F. D. Gac (American Ceramic Society Columbus, OH, 1985) p. 567.
25. L. C. SAWYER, R. T. CHEN, F. HAIMBACK, P. J. HARGET, E. R. PRACK and M. JAFFE, *Ceram. Engng. Sci. Proc.* **7** (1986) 914.
26. S. SHINOZAKI and K. R. KINSMAN, *Mater. Sci. Res.* **11** (1979) 641.
27. O. W. GRIFFIN, D. K. SHETTY, S. Y. LIMAYE and D. W. RICHERSON, *Ceram. Engng. Sci. Proc.* **9** (1988) 671.
28. R. W. GOETTLER and K. T. FABER, *ibid.* **9** (1988) 861.
29. D. B. MARSHALL, *J. Amer. Ceram. Soc.* **67** (1984) C259.
30. F. TUINSTRA and T. L. KOENIG, *J. Compos. Mater.* **4** (1970) 492.
31. H. JEZIVROWSKI and G. STREB, in "11th International Conference on Raman Spectroscopy", edited by R. J. H. Clark and D. A. Long, (Wiley, Chichester, 1988) p. 293.
32. Y. SASAKI, M. SATO, K. OKAMURA and Y. NISHINA, *Sci. Rep. Res. Inst. Tohohu Univ. Ser. A* **32** (1985) 111.
33. D. OLEGO and M. CARDONA, *Phys. Rev.* **B25** (1982) 1151.
34. R. J. DAY, V. PIDDOCK, R. TAYLOR, R. J. YOUNG and M. ZAKIKHANI, *J. Mater. Sci.* **24** (1989) 2898.
35. O. SBAIZERO and A. G. EVANS, *J. Amer. Ceram. Soc.* **69** (1986) 481.

Received 7 August
and accepted 12 October 1992